

## Preparation of G-CuO NPs and G-ZnO NPs with mallow leaves, investigation of their antibacterial behavior and synthesis of bis(indolyl)methane compounds under solvent-free microwave assisted dry milling conditions using G-CuO NPs as a catalyst

Mine SULAK\* 

Department of Mathematics and Science Education, Faculty of Education, Pamukkale University, Denizli, Turkey

Received: 12.05.2021 • Accepted/Published Online: 30.06.2021 • Final Version: 19.10.2021

**Abstract:** In this study, biogenic copper and zinc oxide nanoparticles (G-ZnONPs and G-CuONPs) were synthesized by the green synthesis method using *Malva parviflora* L. (Mallow) leaf extract and the obtained nanoparticles were characterized in detail with UV-Vis, FTIR, SEM, XRD. The antibacterial properties of the synthesized nanoparticles on gram-positive and gram-negative bacteria were investigated and it was found that the nanoparticles had high antimicrobial activity in the results of the experiments. With the obtained G-CuONPs, the synthesis of bis(indolyl)methanes with the “green” one-pot synthesis using microwave was achieved quickly and with high efficiency, and the thermal behavior of the obtained products was investigated.

**Key words:** Indole, green synthesis, microwave reactions, antibacterial, zinc and copper oxide nanoparticles

### 1. Introduction

Nanotechnology is a science that deals with matter at a scale of 1 billionth of a meter (i.e.  $10^{-9}$  m = 1 nm) and is also a field of study related to the manipulation of matter at the atomic and molecular scale [1]. Today, “Nano” is a popular term that is widely used in modern science and is also found in dictionaries: for example, nanoscience, nanowire, nanotube, nanotechnology, nanostructure, nanorobot, and nanomaterial. Nanoparticles have a wide range of use such as energy, physics, chemistry, biology, biotechnology, medicine, industry, technology, and industry [2,3]. Metallic nanoparticles (MNPs) are NPs with sizes between 1 and 100 nm [4]. Recently, impressive advances have emerged in the use of metal nanoparticles over biomolecular interactions, bioassays, biomedical devices, and a variety of other biomedical applications such as immunodiagnosics, drug delivery, therapeutics, and gene therapy. Zinc oxide (ZnO) nanoparticles, the most preferred among metal oxide nanoparticles, are available as white powders and dispersions. ZnO structures have many applications due to their biocompatibility, chemical photochemical stability, wide band gap of 3.37 eV and high binding energy (60 meV) as an important semiconductor [5].

The other nanoparticle used in the study is CuO. Available in different sizes and shapes among various metal oxide nanostructures, CuO is used in many application areas. Examples include sensors, cosmetics, antibacterial activity, chemical absorption, electrical and optical devices, catalysts for liquid phase hydrogenation, and catalyst applications for photocatalytic degradation, biomedical, textile, organic coatings [6–9]. CuO and ZnO nanoparticles are synthesized using chemical and physical methods [10]. Sol-gel process, chemical precipitation, hydrothermal method, microwave, and chemical vapor deposition are among these synthesis methods [11].

However, these methods involve the use of hazardous reagents for the synthesis of nanoparticles and often produce toxic materials that can be harmful to the environment [12, 13]. Therefore, it has become important to produce nanoparticles using low-cost, nontoxic, simple, fast, environmentally friendly methods (green chemistry). At this point, the green-synthesized CuO NPs (G-CuO NPs) and ZnO NPs (G-ZnO NPs) have recently gained increasing attention. The microorganisms used in the green synthesis method include algae, fungi, enzymes, herbs or plant extracts, polyphenols, and flavonoids with strong reducing potential and can act as both reducing and fixing agents in the synthesis process [14–16].

Plants called “medicinal plants” are frequently used in the production of nanoparticles with green synthesis method [17]. One of these medicinal herbs is the mallow plant belonging to the family Malvaceae. One of the mallow species is *M.*

\* Correspondence: msulak@pau.edu.tr

*parviflora* L., which grows mostly in the Aegean and Mediterranean regions. People in Turkey use mallow in the treatment of boils and wounds on the skin, externally as oatmeal porridge, and also for irritation and inflammation of the respiratory and digestive system. The reason why *M. parviflora* L. (Mallow) has these properties is a phytochemical compound called "Malvidine" [18]. In addition, the thymokine phytochemical compounds in the structure of *M. parviflora* L. (Mallow) are involved in the synthesis of nanoparticles.

Heterocyclic compounds are the building blocks of many biologically active substances, which have been studied by many organic chemists. Among such diverse heterocyclic compounds, bis(indolyl)methanes have a special place [19,20]. Indole skeletons can be found as an ingredient in many natural products with high structural complexities and biologically active molecules. As a result, indole and indole derivatives are constantly used in various research fields, e.g., pharmaceuticals, fragrances, agrochemicals, pigments, and materials science. Reserpine, ellipticalin, vincristine, cytotoxic euditalbin, dihydroflustramine, and dipyrromethanes are some examples of indole derivatives. These compounds are used in antitumors, chemotherapy to cure cancer, antimicrobials, and antiparasites. These aforementioned indole derivatives can be obtained through various methods, more specifically, dipyrromethane can be synthesized using several methods. Thus, in the literature, it was reported that there are many synthetic methods to prepare dipyrromethane and its derivatives, such as reacting indole with different aldehydes in the existence of a catalysts like  $H_3PMo_{12}O_{40}$  [21],  $NaBArF_4$  [22],  $La(NO_3)_3 \cdot x6H_2O$  [23],  $Fe(DS)_3$  [24],  $HClO_4$  [25],  $ZrOCl_2 \cdot x8H_2O$  [26],  $BiOClO_4 \cdot xH_2O$  [27],  $ZrO_2$  [28, 29].

Conversely, disadvantages of these methods were reported in the literature as length of reaction time [30,31], high temperature [32,33], **use of expensive catalysts**, or harmful solvent. Use of microwave technology in organic chemistry has been extensively researched in the last two decades, and numerous publications have shown that many chemical syntheses can be successfully carried out with microwave [34,35].

Most importantly, the microwave technique shortens the reaction time considerably, as well as allowing high efficiency, less by-product formation, easier operation in harmony with green chemistry, solvent-free organic transformations, atomic economy, and selective reactions.

Although good results are obtained with both approaches in obtaining indole derivatives, these processes are time consuming. However, in microwave technique, the reaction takes place in a very short time [36].

In the present study, I synthesized CuO and ZnO nanoparticles using mallow plant leaves and examined their antibacterial activities. In addition, I am interested in the study of the synthesis of different substituted dipyrromethane (bis(indolyl) methane) by microwaving technique using CuO nanoparticles as catalysts.

## 2. Materials and methods

### 2.1. Materials

Copper sulphate hexahydrate ( $CuSO_4 \cdot x6H_2O$  99.99 %), zinc acetate hepta hydrate ( $Zn(CH_3COO)_2 \cdot x6H_2O$  99.99 %), sodium hydroxide (NaOH), indole, and aldehyde derivatives were purchased from Germany (Sigma Aldrich Pvt. Ltd. ). As it is of analytical grade, all chemicals were used directly without further purification. The mallow plant (ebegümeçi in Turkish) was collected from fields far from the industrial zone in Pamukkale District of Denizli Province. Bacteria used were obtained from Pamukkale University Biomedical Engineering Department.

### 2.2. Preparation of mallow leaf extracts

Mallow plant leaves were extracted according to the method suggested by Shu [37]. The leaf part of the mallow plant was removed and washed 3 times with deionized water. The leaves were passed through a food processor and divided into small pieces. Twenty grams of mallow leaves and 400 mL of deionized water were added into 1 L of erlenmeyer. This mixture was heated in a magnetic heater at 100 °C for 2 h. The resulting mixture was filtered through Whatman (Grade GF / B: 1.0 µm) filter paper to obtain the extract. The extract was freshly prepared and used in the synthesis phase

### 2.3. Synthesis of copper oxide nanoparticles

Copper oxide nanoparticles were synthesized by the phenolic compounds of the leaf extract through reduction of copper sulphate. By adding 2.6 g of  $CuSO_4 \cdot 5H_2O$  onto 25 mL of mallow extract, the reaction was stirred continuously at 70 °C for 2 h. The pH was adjusted to 11 with 0.1 M NaOH, the reaction mixture changed from dark green to dark brown. The brown solid product was collected by centrifugation at room temperature and washed several times with distilled water. The product was dried overnight at 80 °C and then heated in an oven at 400 °C for 2 h [38].

### 2.4. Synthesis of zinc oxide nanoparticles

In a 100 mL beaker, 20 mL of  $Zn(CH_3COO)_2 \cdot x6H_2O$  solution (10 mM) was added. Next, 5 mL of mallow extract was added dropwise onto this mixture. It was stirred at 80 °C until the color change. The mixture was taken into falcon tubes and centrifuged at 10000 rpm for 10 min. The resulting pellet was washed three times with water to remove organic residues

and then centrifuged again. The pellet part was removed and dried in an oven at 80 °C for 12 h, it was then calcined in an oven at 400 °C. The nanoparticles obtained went through characterization processes and were stored in eppendorf tubes for use in antimicrobial studies [39].

### 2.5. Synthesis of bis(indolyl)methanes by conventional method

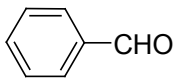

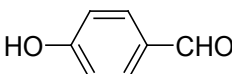
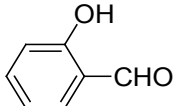
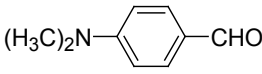

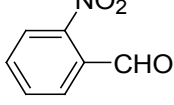
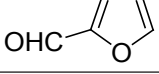
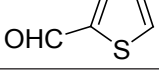
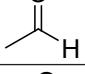
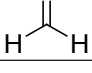
The dipyyromethanes (1a-k, Table 1) were prepared in 80%–91% yields by the condensation of the indole (2 mmol) with the appropriate aryl, alkyl aldehyde (1 mmol) in methanol in the presence of potassium hydrogensulphate (%5 mol). These compounds were isolated as solids and were stable both in solid state and in solution [40].

### 2.6. Synthesis of bis(indolyl)methanes with the microwave method

Benzaldehyde (1 mmol) and indole (2 mmol) were mixed, and G-CuONPs (20 mg) was added. The mixture was ground with a mortar and a pestle until all reactants were completely mixed with each other. The mixture was poured into a beaker, which was then placed in a microwave (LG, MH-4048GW, 480 W, 2 min)

After the reaction was completed, the mixture was allowed to cool to room temperature. We then added approximately 5 mL of ethyl acetate. The CuO nanoparticle was removed by centrifuge, and the ethyl acetate evaporated. Precipitate of

**Table 1.** Physical data of dipyyromethan derivatives and comparative study of conventional vs. microwave method.

Aldehyde	Compound	MP (°C)	Conventional method		MP (°C)	Microwave method	
			Time (min.)	% yield		Time (min.)	% yield
	<b>1a</b>	142–144	90	91	140–142	0.5	99
	<b>1b</b>	193	120	83	194	1	96
	<b>1c</b>	200–210	180	89	210–215	1.5	95
	<b>1d</b>	258	150	88	260	1	97
	<b>1e</b>	203	120	85	200	2	93
	<b>1f</b>	240	210	89	242–245	3	92
	<b>1g</b>	212	180	76	222	2	90
	<b>1h</b>	145–147	120	85	142–144	1.5	94
	<b>1i</b>	125	150	86	127	1.5	99
	<b>1j</b>	100	150	89	98	1	96
	<b>1k</b>	85	120	90	88	1.5	98

the desired compound was recrystallized from ethanol.

**Compound 1a** = Solid; mp 194–196 °C; FTIR (KBr),  $\text{cm}^{-1}$ , nmax: 1031 (C-N), 1460 (Ar-C=C), 2930 (Alif-CH), 3055 (Ar-CH), and 3393 (NH);  $^1\text{H}$  NMR (500 MHz, DMSO-  $d_6$ ): 5.75 (s, 1H, Ar-CH), 6.80 (s, 2H, Ar-H), 7.00 (t, 2H, Ar-H), 7.15–7.28 (m, 10H,  $J_{\text{H}} 8.1$  Hz, Ar-H), 10.9 (s, 2H, NH).

**Compound 1b** = Solid; mp 194 °C; FTIR (KBr),  $\text{cm}^{-1}$ , nmax: 1250 (C-O-C), 1420 (C-N), 1510–1620 (Ar-C=C), 2890 (Ar-OCH<sub>3</sub>), 3060 (Ar-CH), and 3390 (NH);  $^1\text{H}$  NMR (500 MHz, DMSO-  $d_6$ ): 3.68 (s, 3H, O-CH<sub>3</sub>), 5.85 (s, 1H, Ar-CH), 6.64 (s, 6H, Ar-H), 6.83(d, 2H, Ar-H) 7.00 (t, 2H, Ar-H), 7.12 (t, 2H, Ar-H), 7.30–7.38 (dd, 2H,  $J_{\text{H}} 8.1$  Hz, Ar-H), 10.86 (s, 2H, NH).

**Compound 1c** = Solid; mp 210–215 °C; FTIR (KBr),  $\text{cm}^{-1}$ , nmax: 1220 (C-O), 1459 (C-N), 1500–1616 (Ar-C=C), 3054 (Ar-CH) and 3410 (NH), 3600 (OH);  $^1\text{H}$  NMR (500 MHz, DMSO- $d_6$ ): 5.72 (s, 1H, Ar-CH), 6.58 (s, 2H, 8.5 Hz, Ar-H), 6.83 (t, 2H,  $J_{\text{H}} 1.8$  Hz, Ar-H), 7.06 (t, 2H, Ar-H), 7.20–7.34 (m, 8H,  $J_{\text{H}} 7.9$  Hz, Ar-H), 9.21 (s, 2H, NH), 10.5 (s, 1H, OH).

**Compound 1d** = Solid; mp 260 °C; FTIR (KBr),  $\text{cm}^{-1}$ , nmax: 1240 (C-O), 1455 (C-N), 1490–1699 (Ar-C=C), 3050 (Ar-CH) and 3420 (NH);  $^1\text{H}$  NMR (500 MHz, DMSO- $d_6$ ): 6.20 (s, 1H, Ar-CH), 6.78–7.12 (m, 9H, Ar-H), 7.32 (dd, 4H,  $J_{\text{H}} 7.8$  Hz, Ar-H), 7.38 (dd, 1H,  $J_{\text{H}} 8.2$  Hz, Ar-H), 9.48 (s, 2H, NH), 10.87 (s, 1H, OH).

**Compound 1e** = Solid; mp 200 °C; FTIR (KBr),  $\text{cm}^{-1}$ , nmax: 1190 (Ar-N), 1465 (C-N), 1599 (Ar-C=C), 3070 (Ar-CH) and 3430 (NH);  $^1\text{H}$  NMR (500 MHz, DMSO- $d_6$ ): 2.91 (s, 6H, CH<sub>3</sub>), 5.71 (s, 1H, Ar-CH), 6.71 (d, 2H,  $J_{\text{H}} 8.7$  Hz, Ar-H), 6.83 (d, 2H,  $J_{\text{H}} 2.0$  Hz, Ar-H), 6.91 (s, 2H, Ar-H), 7.11 (s, 2H, Ar-H), 7.21 (d, 2H,  $J_{\text{H}} 8.6$  Hz, Ar-H), 7.31 (d, 2H,  $J_{\text{H}} 7.9$  Hz, Ar-H), 7.37 (d, 2H,  $J_{\text{H}} 8.1$  Hz, Ar-H), 10.89 (s, 2H, NH).

**Compound 1f** = Solid; mp 242–244 °C; FTIR (KBr),  $\text{cm}^{-1}$ , nmax: 1259 (C-N), 1352 (N-O), 1540 (Ar-N), 1598–1616 (Ar-C=C), 3049 (Ar-CH) and 3451 (NH);  $^1\text{H}$  NMR (500 MHz, DMSO- $d_6$ ): 6.00 (s, 1H, Ar-CH), 6.91 (s, 2H, Ar-H), 7.09–7.15 (m, 3H, Ar-H), 7.32 (d, 3H,  $J_{\text{H}} 8.0$  Hz, Ar-H), 7.40 (d, 2H,  $J_{\text{H}} 8.1$  Hz, Ar-H), 7.73 (d, 2H,  $J_{\text{H}} 8.7$  Hz), 8.22 (d, 2H,  $J_{\text{H}} 8.7$  Hz, Ar-H), 10.9 (s, 2H, NH).

**Compound 1g** = Solid; mp 222 °C; FTIR (KBr),  $\text{cm}^{-1}$ , nmax: 1245 (C-N), 1348 (N-O), 1481–1614 (Ar-C=C), 3065 (Ar-CH) and 3448 (NH);  $^1\text{H}$  NMR (500 MHz, DMSO- $d_6$ ): 6.4 (s, 1H, Ar-CH), 6.67 (dd, 2H, Ar-H), 7.04 (dt, 2H, Ar-H), 7.24 (dt, 2H,  $J_{\text{H}} 7.4$  Hz, Ar-H), 7.3 (d, 2H,  $J_{\text{H}} 8.12$  Hz, Ar-H), 7.49 (d, 2H,  $J_{\text{H}} 7.12$  Hz, Ar-H), 7.59 (t, 1H, Ar-H), 7.61 (d, 1H,  $J_{\text{H}} 7.8$  Hz, Ar-H), 8.01 (dq, 1H,  $J_{\text{H}} 8.7$  Hz, Ar-H), 8.23 (dq, 1H,  $J_{\text{H}} 8.7$  Hz, Ar-H), 10.5 (s, 2H, NH).

**Compound 1h** = Solid; mp 142–144 °C; FTIR (KBr),  $\text{cm}^{-1}$ , nmax: 1461–1620 (Ar-C=C), 1709 (C-O), 3058 (Ar-CH) and 3421 (N-H);  $^1\text{H}$  NMR (500 MHz, DMSO- $d_6$ ): 5.89 (s, 1H, Ar-CH), 6.17–7.10 (m, 5H, Ar-H) 7.21–7.31 (m, 6H, Ar-H), 7.41 (d, 2H,  $J_{\text{H}} 8.1$  Hz, Ar-H), 9.8 (s, 2H, NH).

**Compound 1i** = Solid; mp 127 °C; FTIR (KBr),  $\text{cm}^{-1}$ , nmax: 600 (Ar-S), 1451–1622 (Ar-C=C), 1719 (C-S), 3034 (Ar-CH) and 3420 (N-H);  $^1\text{H}$  NMR (500 MHz, DMSO- $d_6$ ): 6.1 (s, 1H, Ar-CH), 6.83–6.95 (m, 4H, Ar-H), 7.0–7.13 (m, 4H, Ar-H), 7.30 (dd, 1H,  $J_{\text{H}} 3.6$  Hz, Ar-H), 7.37 (dd, 4H,  $J_{\text{H}} 11.4$  Hz, Ar-H), 8.5 (s, 2H, NH).

**Compound 1j** = Solid; mp 98 °C; FTIR (KBr),  $\text{cm}^{-1}$ , nmax: 1381 (CH<sub>2</sub>), 1456–1630 (Ar-C=C), 2910 (CH<sub>3</sub>), 3050 (Ar-CH) and 3431 (N-H);  $^1\text{H}$  NMR (500 MHz, DMSO- $d_6$ ): 1.6 (d, 3H, CH<sub>3</sub>-CH), 4.5 (q, 1H,  $J_{\text{H}} 7.3$  Hz, CH-CH<sub>3</sub>), 7.0 (m, 2H,  $J_{\text{H}} 6.9$  Hz, Ar-H), 7.2 (m, 2H,  $J_{\text{H}} 8.1$  Hz, Ar-H), 7.41 (dd, 2H, Ar-H), 7.67 (d, 2H, Ar-H), 8.3 (s, 2H, NH).

**Compound 1k** = Solid; mp 88 °C; FTIR (KBr),  $\text{cm}^{-1}$ , nmax: 1430 (CH<sub>2</sub>), 1610 (Ar-C=C), 3100 (Ar-CH) and 3490 (N-H);  $^1\text{H}$  NMR (500 MHz, DMSO- $d_6$ ): 4.20 (s, 2H, CH<sub>2</sub>), 6.88 (m, 2H, Ar-H), 7.00 (m, 2H, Ar-H), 7.20 (d, 2H,  $J_{\text{H}} 2.0$  Hz, Ar-H), 7.40 (d, 2H,  $J_{\text{H}} 8.0$  Hz, Ar-H), 7.65 (d, 2H,  $J_{\text{H}} 7.9$  Hz, Ar-H), 8.1 (s, 2H, NH).

## 2.7. Characterization methods of compounds

### 2.7.1. Characterization methods of nanoparticles

The synthesized NPs were enclosed in a quartz cuvette and the absorbance was measured in the wavelength range of 200 to 800 nm using a UV-Vis spectrophotometer (UV / Vis-1601, Shimadzu, Kanagawa, Japan) adjusted to a resolution of 1 nm.

Fourier transform infrared spectroscopy (FTIR) shows the presence of bio-organic components that act as a possible stabilizer for synthesized NPs. After the synthesis of the NPs, biomolecules associated with it were identified by FTIR measurements.

G-CuONPs and G-ZnONPs were subjected to FTIR analysis. The samples were exposed to an infrared source with the spectrum scanned in the 400–4000  $\text{cm}^{-1}$  range to achieve good signal to noise ratio. Various vibration modes have been identified and assigned to identify different functional groups on the NPs.

Chemical composition analysis and morphology of the synthesized NPs were performed using an energy-dispersive X-ray spectroscopy (EDX) analyzer associated with a scanning electron microscope (SEM) (Zeiss Supra 40 VP). A very small sample of the synthesized and stabilized NPs was prepared on a carbon-coated copper grid, and then SEM imaging was taken by coating with a layer of gold-palladium using the spray coater (Quorum Q150R ES, Quorum Technologies Ltd, UK).

The nanoparticle powder obtained was analyzed using an ADP PRO 2000 X-ray diffraction system with Cu K $\alpha$  radiation ( $\lambda = 1.54059 \text{ \AA}$ ). The XRD pattern was studied with a 0.02 step size in the  $2\theta$  range between  $5^\circ$  and  $90^\circ$ . The area size of the crystal was calculated using the Debye–Scherrer formula [41].

### 2.7.2. Characterization methods of bis(indolyl)methane derivatives

Melting points were measured on an electrothermal digital microscopic melting point apparatus and recorded without modification. The reaction was followed by thin layer chromatography on silica.  $^1\text{H}$  NMR and  $^{13}\text{C}$  NMR spectra were recorded with tetramethylsilane as standard in  $\text{CDCl}_3$  or  $\text{DMSO-}d_6$  solution, respectively, using a Bruker AMX 500-MHz spectrometer at 500 and 125 MHz. Chemical shifts were measured in parts per million (ppm) and coupling constants (J), hertz (Hz).

Low resolution mass spectrographic analyses were measured using the electrospray ionization technique on a Bruker Esquire 3000 spectrometer. Thermogravimetry (TG), differential thermogravimetry (DTG), and differential thermal analysis (DTA) curves were obtained simultaneously using a Shimadzu DTG-60H thermal analyzer. The air atmosphere was selected and the flowing rate was adjusted as  $25 \text{ mL min}^{-1}$ , since the potential applications of these compounds were carried out in air. All compounds were heated from room temperature to  $800^\circ\text{C}$  with using  $10^\circ\text{C min}^{-1}$  heating rate. Silver was used to calibrate the balance for buoyancy effects for the quantitative estimation of mass change. The melting points indium of tin (provided by Shimadzu) were used to calibrate the temperature. Four different compounds (**1a**, **1b**, **1d**, **1h**) were selected for thermal investigation. These compounds were chosen due to the varied functional groups.

### 2.8. Antimicrobial activity

In this study, the antimicrobial activity of nanoparticles was defined on three gram- negative and five gram-positive bacteria using disk diffusion method according to Clinical Laboratory Institute standard<sup>1</sup>

Paper discs impregnated with certain amounts of G-CuONPs and ZnO NPs were placed in solid media with a high concentration of the microorganism to be tested using a pair of sterile forceps. During this process, it has been paid attention that there is a distance of 22 mm between the discs and 14 mm from the edge of the petri dish so that the zones to be formed do not overlap each other. Media were incubated for 18–24 h at  $35^\circ\text{C}$ . The diameter of the inhibition zone was measured in millimeters and evaluations were made according to standard tables.

### 3. Results and discussion

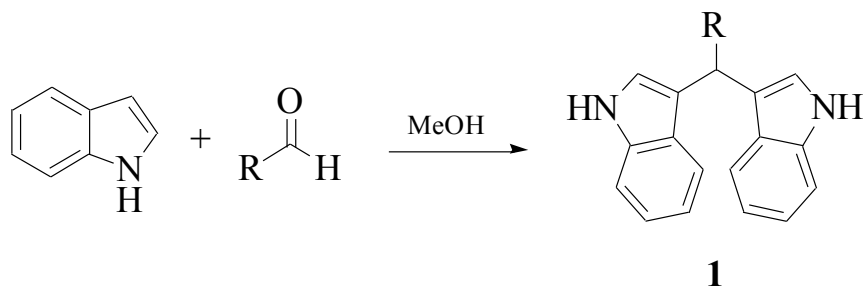
Dipyyromethane (bis(indolyl)methane) was synthesized using both conventional methods and microwaves, and the same material was used in both conditions.

Traditional synthesis methods in organic chemistry require a longer heating period and therefore also require an exhaustive and tiresome apparatus set-up which results in a higher cost and environmental pollution (Figure 1). Additionally, the synthesis process requires large quantities of toxic chemicals and solvents for reactions. Reactions with microwave are a study of “green chemistry” performed in closed containers at high temperatures with low-boiling solvents (Figure 2). Green processes use less catalysts and readily recyclable solvents or media and often yield more products than normal. When the reactions with microwave and traditional organic chemistry were compared, it was observed that the product yield increased by 10%–30% compared to traditional methods. Each reaction was repeated at least three times (with different time intervals). Comparative results regarding the products’ melting points and percentage yields are presented in Table 1. The reaction with indoles has been demonstrated using various substituted aromatic and aliphatic aldehydes. Bis(indolyl)methanes were obtained in 90% and higher yields. The substituents in the aromatic ring, whether electron withdrawing or electron donating, (these substituent groups were in the o-, m-, p- positions on the ring) did not show any visible effect on the formation of the bis(indolyl)methane compound, and the products were obtained with high yield.

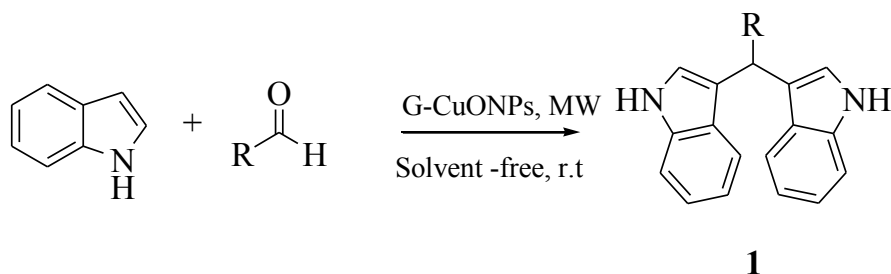
Especially in medicinal plants, there are many metabolites with pharmacological activity. Many studies have shown that these metabolites become more effective by binding to the synthesized nanoparticles and add more properties to nanoparticles [42]. Another advantage of the green synthesis of nanoparticles is that while some functional groups must be added to the surface of nanoparticles in physicochemical synthesis, this step is not necessary for nanoparticles synthesized in biological ways [43]. In addition, the time required for the biosynthesis of nanoparticles is shorter than the time required for physicochemical approaches. As a result of the interaction of plant extract and metal (Cu, Zn) salts, the color changes occurring in the reaction medium and metal oxide nanoparticles were obtained (Figure 3).

UV-Visible spectroscopy was used to examine the optical properties of CuO and ZnO nanoparticles obtained as a result of experimental studies. In Figures 4a and 4b, UV-Visible spectra of CuO and ZnO nanoparticles prepared by green synthesis are given. Transition type and band gap value can be determined from absorption bands in UV-Visible spectroscopy [44,45].

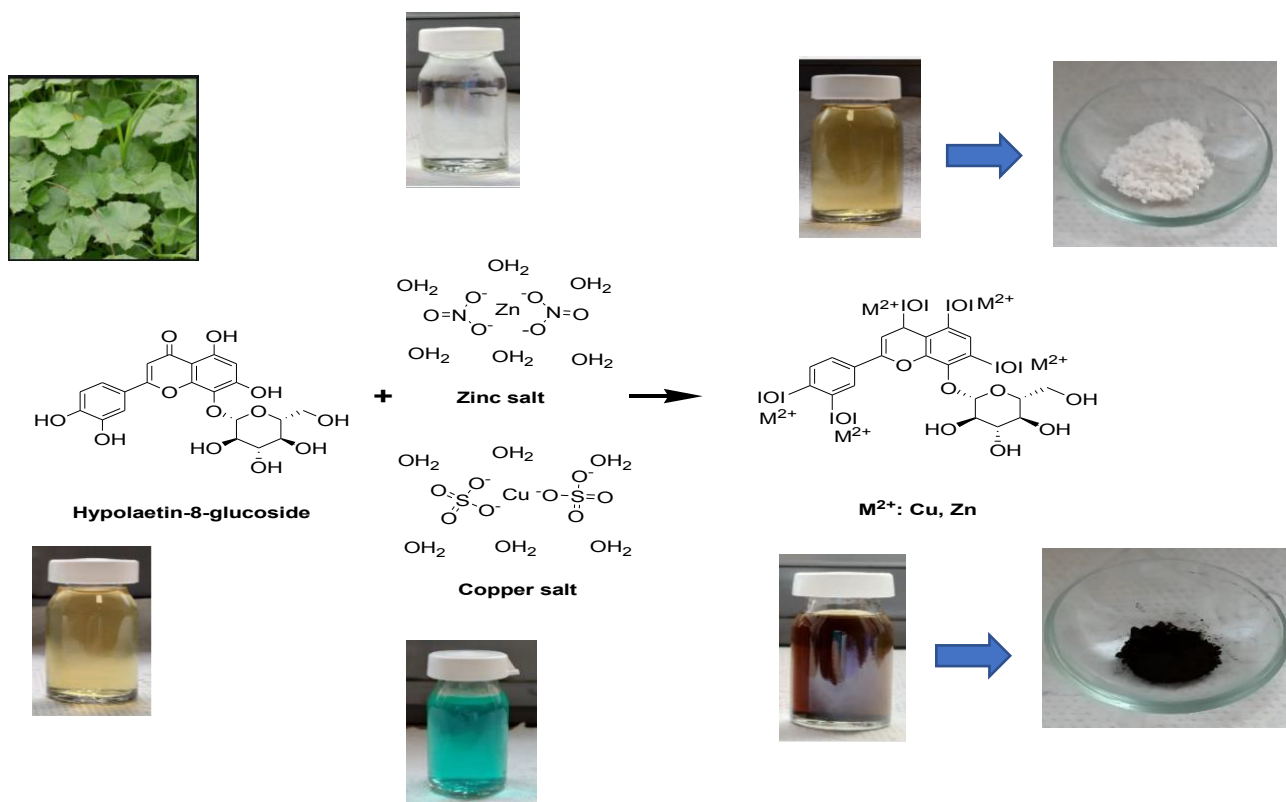
<sup>1</sup> Anonymous (2020). M100 | Performance Standards for Antimicrobial Susceptibility Testing, 31st Edition, Clinical Laboratory Institute [online]. Website <https://clsi.org/>



**Figure 1.** Conventional methods of synthetic reactions.



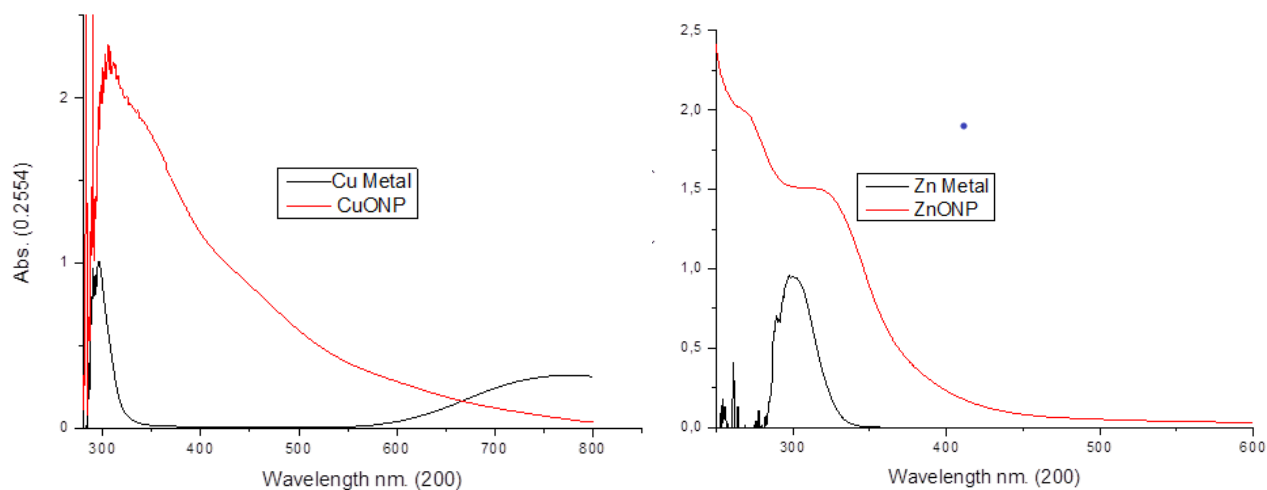
**Figure 2.** Microwave methods of synthetic reactions.



**Figure 3.** Bioextract of the mallow plant, Zn, Cu salt solution, G-CuONPs and G-ZnONPs solution.

A characteristic absorption peak at 360 nm wavelength is given in the UV-Visible spectrum of G-ZnO nanoparticles in Figure 4b. This base band absorption of ZnO is due to electron transitions from the valence band to the conducting band.

The band gap energy ( $E$ ) of the prepared CuO and ZnO nanoparticles was calculated using the following equation (Equation 1) [46].



**Figure 4.** UV-Vis spectrum of ZnO and CuO nanoparticles.

$$E = h \times C/\lambda$$

(1)

Here, E = Band gap energy

h = Planck's constant =  $6.626 \times 10^{-34}$  Joule sec

C = Speed of light =  $3.0 \times 10^8$  meters / s  $\lambda$  = Cut wavelength =  $299 \times 10^{-9}$  meters (ZnO)  $294 \times 10^{-9}$  meters (CuO)

\* Conversion  $1\text{eV} = 1.6 \times 10^{-19}$  Joules

The band gap energy (E) of the prepared ZnO and CuO nanoparticles were calculated using equation (1). The calculated band gap energy value of ZnO nanoparticles is 4.16 eV. It reveals that ZnO nanoparticles can be used in medical applications such as sunscreens or antiseptic ointments due to their intense absorption in the UV region. The band gap energy of the CuO nanoparticle obtained by the green synthesis method from the mallow plant is 4.22 eV. Since the G-CuO NPs energy band gap is more than 4 eV, it can be used as a photocatalyst.

FTIR analysis performed to characterize the surface structure of G-CuNPs is shown in Figure 5a. The visible bands belong to the functional groups of biomolecules adsorbed on NPs. FTIR spectra of G-CuNPs exhibited vibrations in the region of  $500\text{--}600\text{ cm}^{-1}$  that can be attributed to Cu vibrations confirming the formation of G-CuNPs. Depending on the vibrations of Cu, an absorption band was observed at  $625\text{ cm}^{-1}$ . A dense and wide band of  $3303\text{ cm}^{-1}$  emerged in the region corresponding to the stretching movements of hydroxyl functional groups [47]. Metal-oxygen (Cu-O) band vibrations were determined at  $515\text{ cm}^{-1}$ .

In the FTIR spectra of the synthesized ZnO nanoparticle, a strong band was observed at  $470\text{ cm}^{-1}$ . It has been reported in the literature that this absorption band belongs to the characteristic vibration of the Zn-O bond (Figure 5b). When the FTIR spectra of G- ZnO NPs given in the literature were examined, it was determined that the FTIR spectra obtained were compatible with the spectra given in the literature [48].

SEM images of synthesized ZnO nanoparticles are given in Figure 6a. When SEM images are examined, it is seen that the produced ZnO particles generally have a hexagonal morphological structure. ZnO nanoparticles obtained by the green synthesis method have an average diameter of 64.5 nm.

When the SEM images were examined, it was observed that the synthesized G-CuONPs had spherical shapes. It was observed that the particle sizes for the synthesized G-CuONPs were in the range of 42.2–47.2 nm (Figure 6b).

EDX analysis was performed to examine the elemental composition of metal oxide nanoparticles obtained as a result of experimental studies. EDX analysis of CuO and ZnO nanoparticles obtained are given in Figures 7a and 7b.

Theoretically, the atomic percentage of metals (Cu and Zn) and oxygen should be 50% each. As seen in Figure 7a, as a result of the analysis, it was determined that the atomic copper percentage was 50% and the oxygen percentage was 50%. As can be seen in Figure 7b, as a result of the analysis, it was determined that the atomic percentage of zinc and oxygen were 50% and 50%, respectively. When looking at EDX analysis of both metal oxide nanoparticles, it is seen that they are stoichiometric and compatible with theoretical values.

According to the results of XRD analysis, it was determined according to the ICDD library that the peaks belong to the monoclinic CuO nanoparticles, and the mesh parameters were  $a = 4.687\text{ \AA}$   $b = 3.422\text{ \AA}$   $c = 5.130\text{ \AA}$  (ICDD card no: 01-089-5897). The average particle size calculated according to the Debye-Scherrer formula is approximately 25 nm. In Figure 8a, the X-ray diffractogram of the G-CuONPs sample is given with Miller indices (orientation planes).

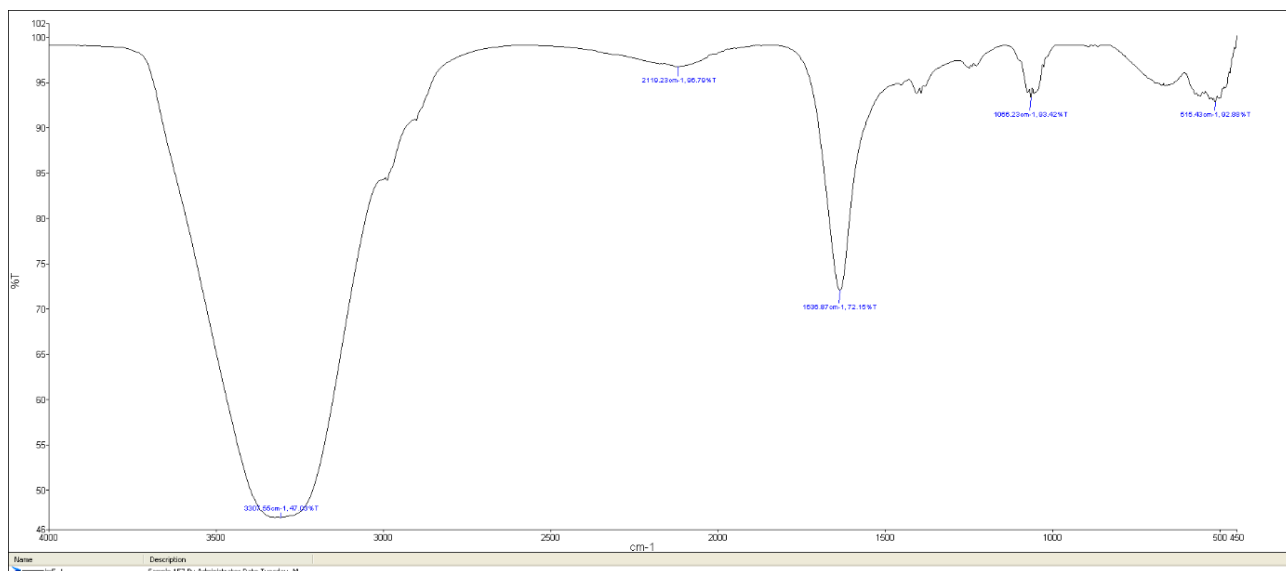


Figure 5a . FTIR analysis of CuO nanoparticles.

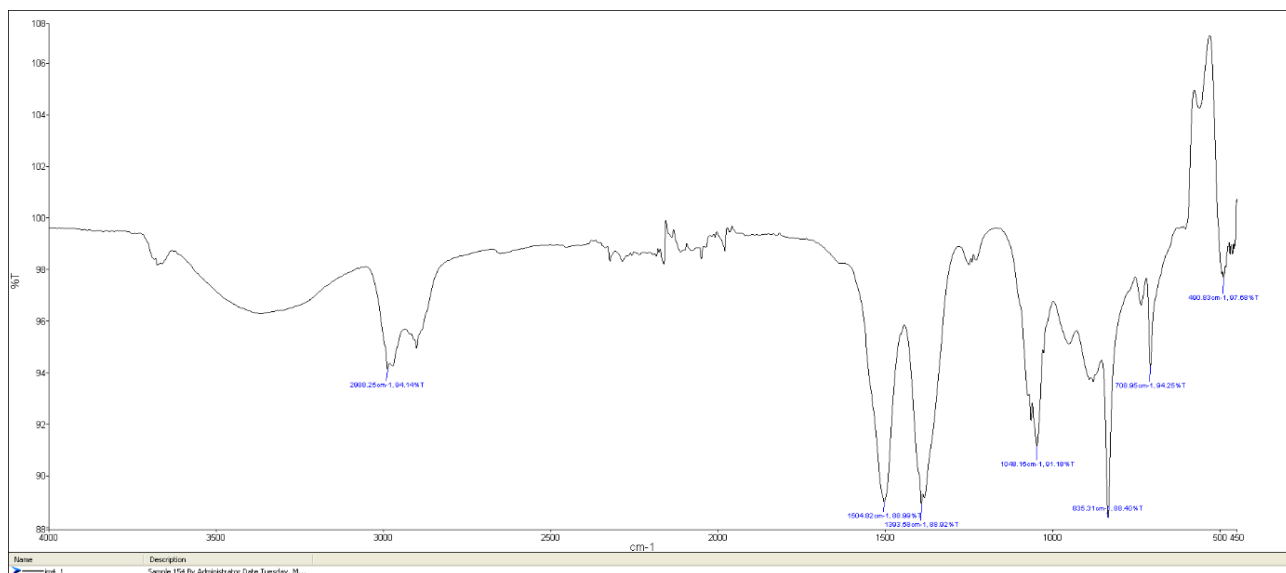


Figure 5b. FTIR analysis of ZnO nanoparticles.

ZnO structural characterization using X-ray diffractometry has been made. Figure 8b shows the XRD diffraction pattern of ZnO nanoparticles prepared by biosynthesis method. Diffraction peaks at  $a=3,250 \text{ \AA}$  ve  $c=5,207 \text{ \AA}$   $2\theta$  correspond to the (100), (002) and (101) planes, respectively, confirming that ZnO has a hexagonal structure. There are no peaks attributable to any impurities and the expansion of the peaks, and this confirms that the synthesized ZnO nanoparticles are highly pure nanocrystal. The average particle size calculated according to the Debye–Scherrer formula is approximately 31.38 nm.

Four different compounds (**1a**, **1b**, **1d**, **1h**) were selected to examine the thermal decomposition stages and to compare thermal stability in this part of the study. It was found that thermal stabilities of compounds vary depending on the substituted groups. Compound **1b** shows the highest thermal stability and starts to decompose after 175 °C. However, compound **1a** shows the lowest thermal stability and starts to decompose after 130 °C. The thermo-analytical results are summarized in Table 2.

The first three compounds (**1a**, **1b**, **1d**) show similar thermal behavior. TG and DTA curves of these compounds are given in Figure 9. These compounds decompose with three exothermic stages. The first stages correspond to the removal of aldehyde groups. Experimental mass loss values (23.358, 29.549, and 27.680, respectively) of these stages are compatible



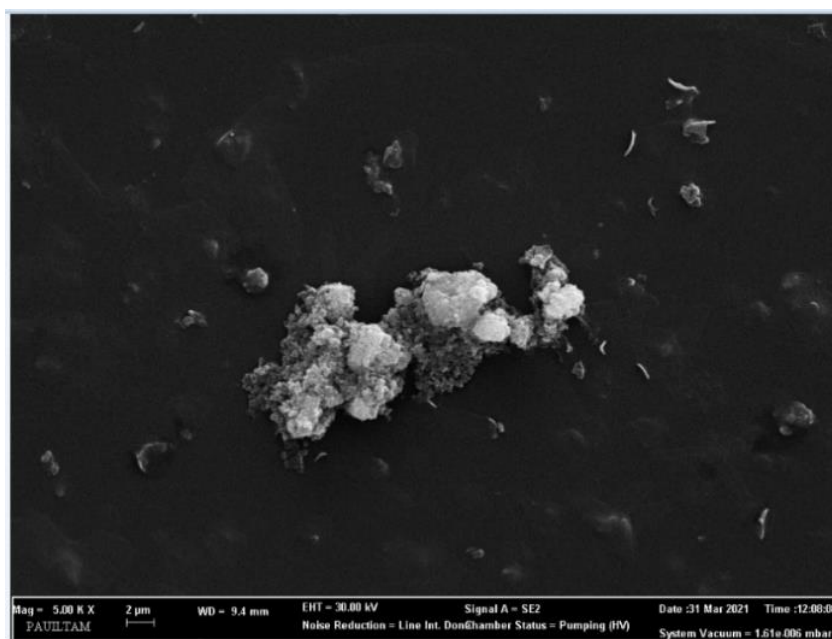


Figure 6a. SEM image of ZnO nanoparticles.

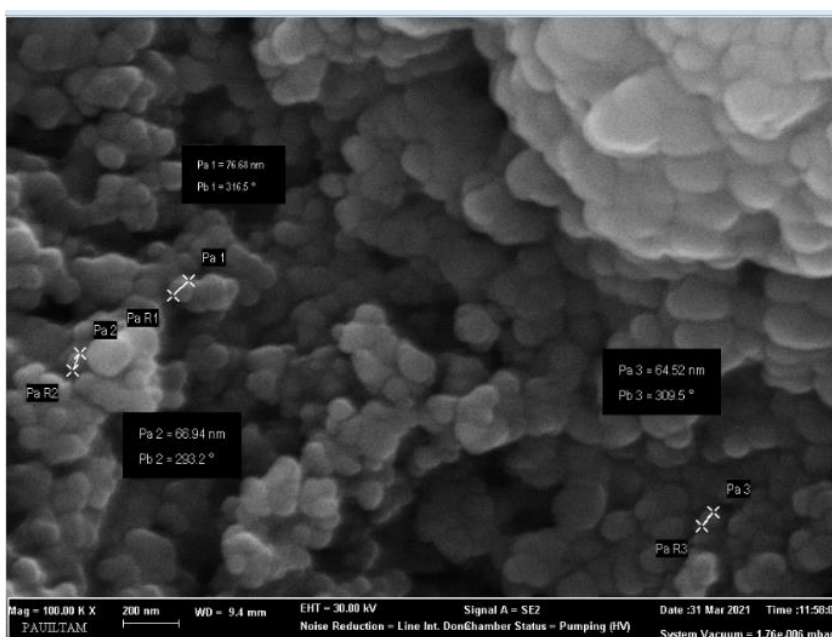
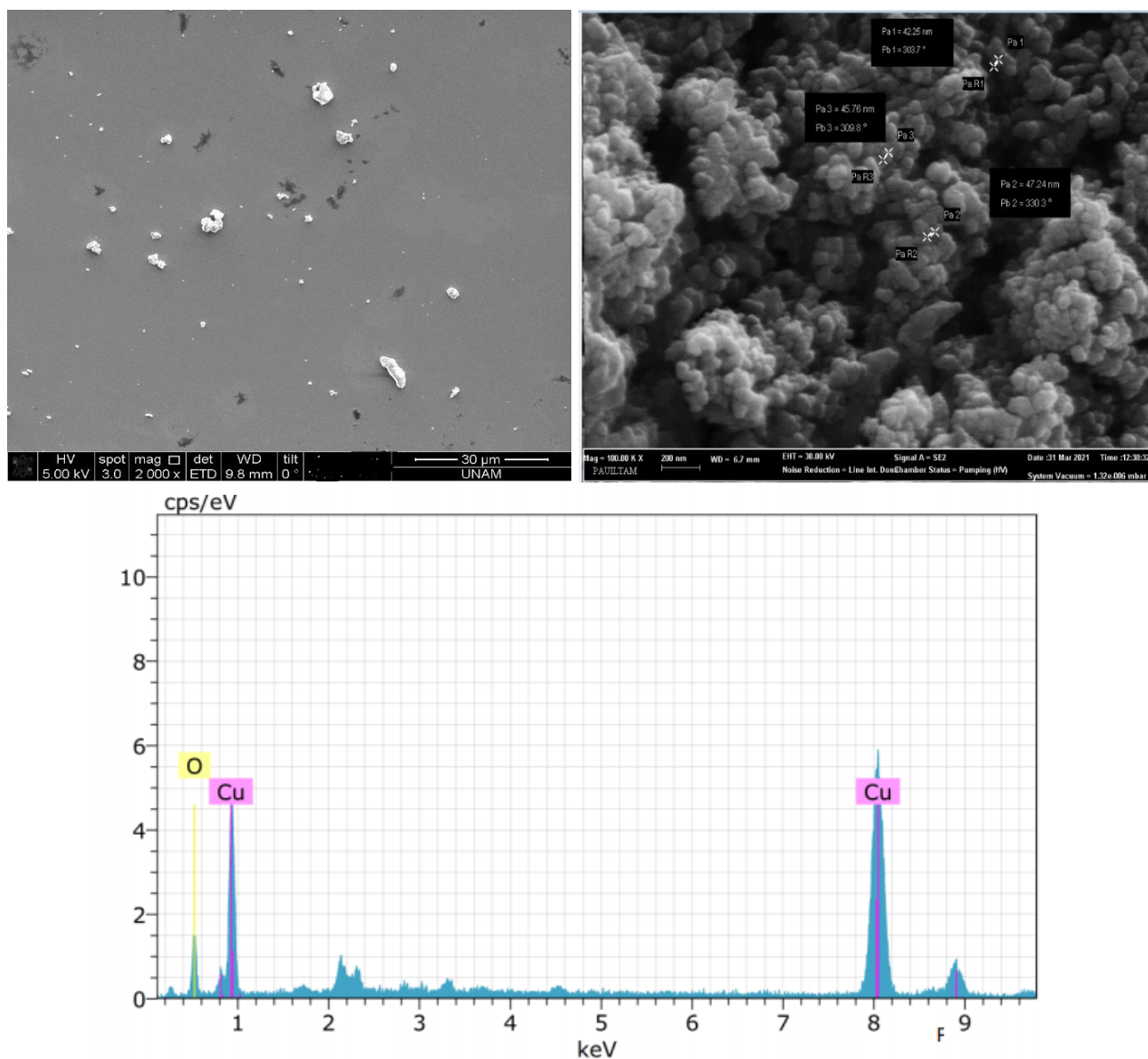


Figure 6b. SEM image of CuO nanoparticles.

with theoretical mass loss values (23.602, 30.114, 34.319). One indole group degrades from the structure at the second stage. The average reaction interval of this degradation is 363–570 °C. Finally, the rest of the structure is decomposed. Peak temperature of this stage is observed as 628.44, 541.71, and 613.53 °C, respectively. Differently from compounds **1a** and **1d**, an endothermic peak was observed in the DTA curve of compound **1b**. This peak belongs to melting and shows a maximum at 193.94 °C.

The TG and DTA curves of **1h** compounds are presented in Figure 10. The decomposition mechanism of this compound shows differences compared to the other three compounds. Decomposition proceeds with two exothermic stages. The first stage corresponds to the degradation of one indole group and occurs in the 147–479 °C temperature range, with 37.738%



**Figure 7a.** EDX spectrum of CuONp synthesized with bioextract.

experimental mass loss. The second stage starts immediately after the completion of first stage and the decomposition of all structures continues. Exothermic characters of this stage are higher than the first reaction stage. The reaction peak temperature is 507.23 °C.

Thermal stabilities and decomposition mechanisms of four bis(indolyl)methanes compounds were compared. As a result of these comparisons, we concluded that the thermal stability of the compounds depended on substituted groups and their positions. Determination of thermal stability of these compounds is very important for potential usage areas.

This experiment was carried out using solvent-free reaction conditions, various benzaldehyde derivatives, and indoles that reacted with CuO nanoparticle which is inexpensive and stable. In addition to the aromatic aldehyde, aliphatic aldehyde was used and obtained excellent results were obtained in aliphatic aldehydes. After completion of the reaction, the reaction mixture ethyl acetate (5 mL) and G-CuONPs were recovered by centrifuge, washing with methanol, and drying in a vacuum used in other reactions without losing effectiveness. I examined the synthesis of bis(indolyl)methanes performed both with the conventional method and the microwave method. I have found that, with the microwave method, products are obtained with higher efficiency and higher purity, greater reproducibility, lower energy use in a convenient, cleaner, and efficient way, and the synthetic protocol is efficient for using G-CuONPs under solvent-free conditions.

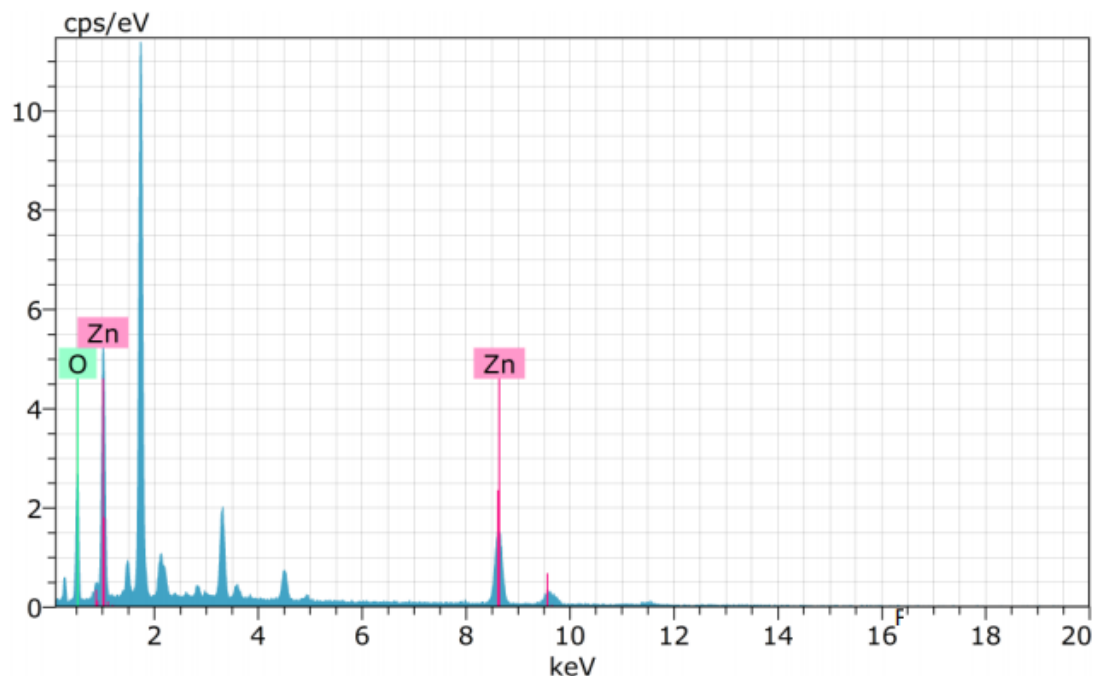


Figure 7b. EDX spectrum of ZnONp.

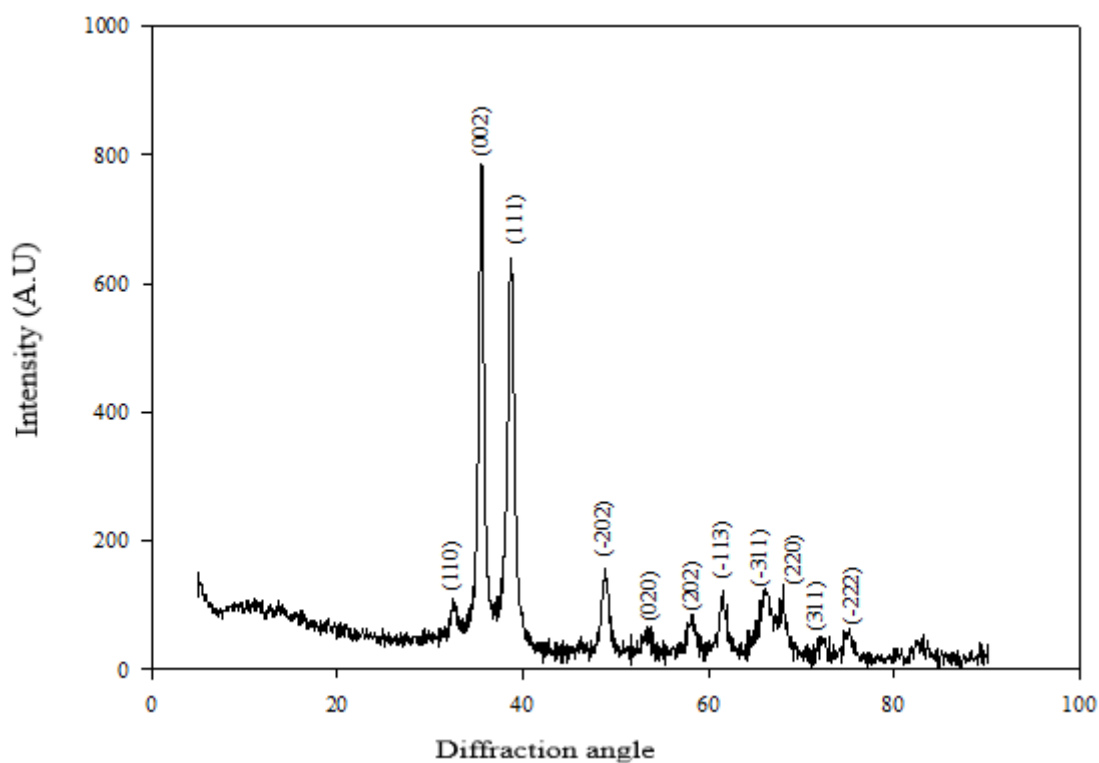
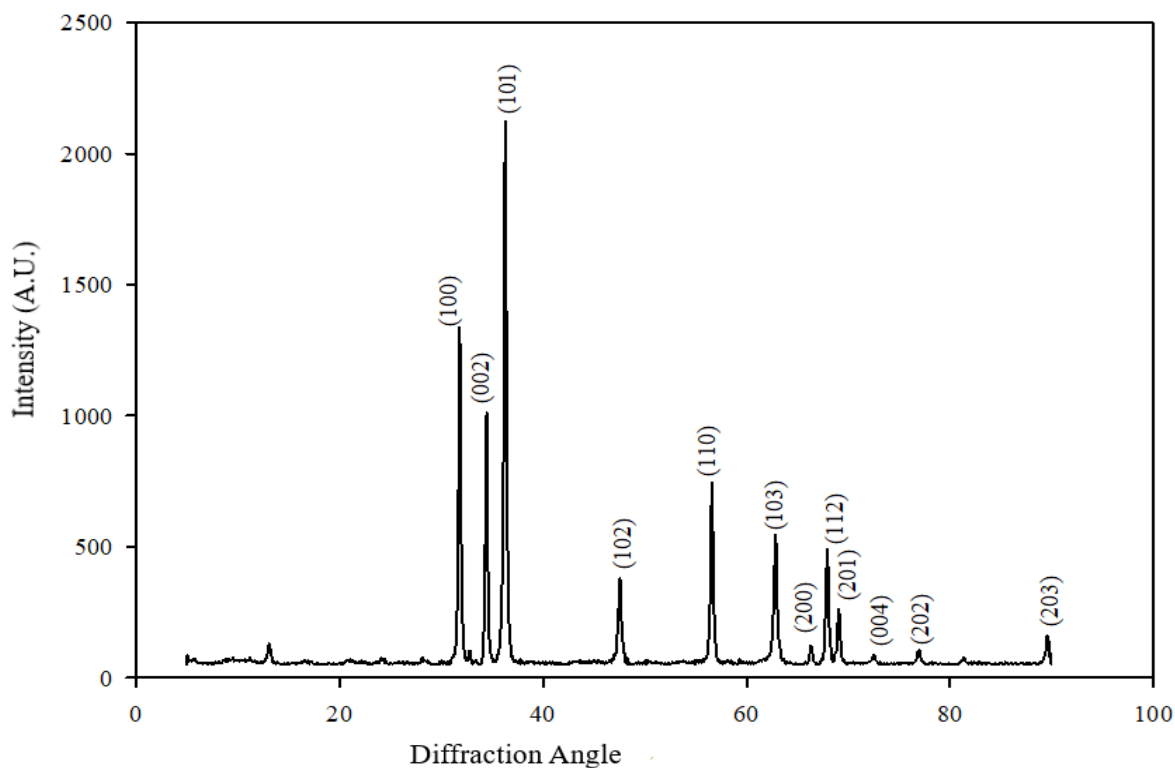


Figure 8a. X-Ray Diffractogram / Diffraction Pattern of nano CuO compound derived from malow plant

#### 4. Antibacterial studies

Research has shown that bio-synthesized nanoparticles have higher antimicrobial activity compared to chemically synthesized nanoparticles. Mukherjee et al. reported that biological nanoparticles showed 96.67% antibacterial activity, but chemically synthesized nanoparticles did not show a significant effect on antibacterial activity [48].



**Figure 8b.** X-Ray Diffractogram / Diffraction Pattern of nano ZnO compound derived from malow plant

**Table 2.** The thermoanalytical results of all compounds (*1a*, *1b*, *1d*, *1h*).

<i>Compound</i>	$T_i-T_f/^\circ\text{C}$		$T_{peak}/^\circ\text{C}$	<i>Mass loss%</i> <sup>(exp.)</sup>	<i>Mass loss%</i> <sup>(theo.)</sup>
<i>1a</i>	130–305		287.77	23.358	23.602
	305–587		523.99	37.116	36.602
	587–802		628.44	43.371	39.796
<i>1b</i>	175–321		307.89	29.549	30.114
	321–527	419.58	31.953	32.954	
	527–667	541.71	36.932	40.664	
<i>1d</i>	161–462	230.42	27.680	27.219	
	462–597	535.05	35.072	34.319	
	597–654	613.53	34.319	39.552	
<i>1h</i>	147–479	318.09	37.738	37.179	
	479–630	507.23	62.821	67.417	

As mentioned earlier, antibacterial properties of CuO and ZnO nanoparticles, three gram-positive bacteria (*B. subtilis*, *S. aureus*, *B. cereus*) and five gram-negative (*K. pneumoniae*, *V. parahaemolyticus*, *E. coli*, *S. typhimurium*, *S. enteritidis*) were investigated using disk diffusion method against six bacterial strains. The antibacterial effects of ZnO and CuO nanoparticles against bacteria are given in Table 3.

In this study, in vitro susceptibilities of CuO and ZnO nanoparticles synthesized by green synthesis method against gram-positive and gram-negative bacteria were determined using disk diffusion methods. For two different nanoparticles, it was observed that it has different microbial activity against different bacteria at varying rates between 2 mm and 21

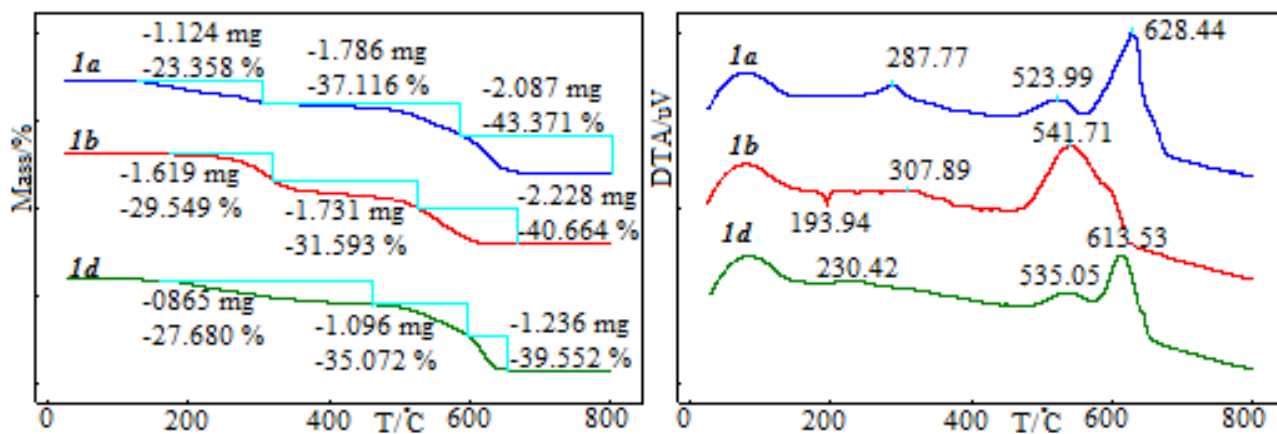


Figure 9. The TG and DTA curves of *1a*, *1b*, *1d* compounds.

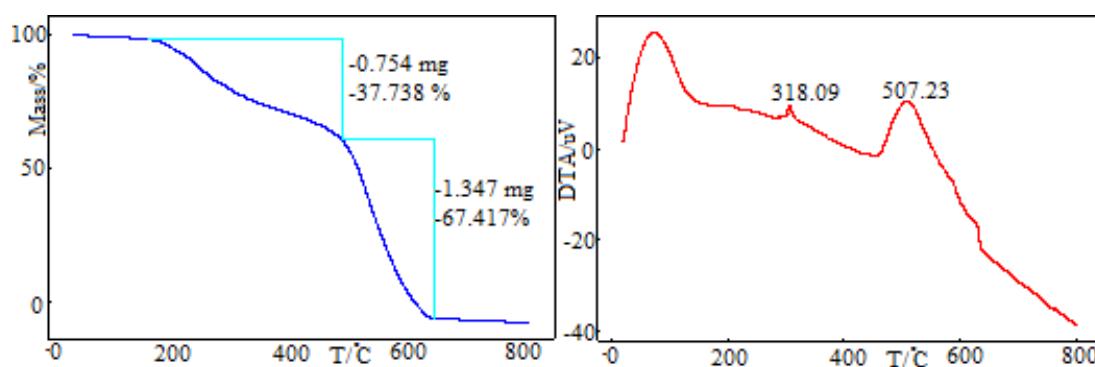


Figure 10. The TG and DTA curves of *1h* compound.

Table 3. Inhibition zones formed by G-CuONPs and G-ZnONPs.

	<i>K. pneumoniae</i>	<i>V. parahaemolyticus</i>	<i>E. coli</i>	<i>S. typhimurium</i>	<i>S. enteritidis</i>	<i>B. subtilis</i>	<i>S. aureus</i>	<i>B. cereus</i>
CuO	3	13	14	2	4	11	2	8
ZnO	18	21	10	13	19	19	13	13

mm. In the disk diffusion test, the largest zone diameter for bacteria was measured against *V. parahaemolyticus* with a diameter of 21 mm using the ZnO nanoparticle (Figure 11). *Vibrio parahaemolyticus* is observed with a maximum zone diameter while the zone diameter is small against CuO nanoparticles *Klebsiella pneumoniae*, *Salmonella typhimurium*, and *Salmonella enteritidis*. Differences in sensitivity and resistance to both gram-positive and gram-negative bacterial populations may be due to differences in cell structure, physiology, metabolism, or the degree of contact of organisms with nanoparticles. In addition, other factors such as nanoparticle diffusion rate may affect the bacterial strain differently [49].

## 5. Conclusions

Many researchers have published studies on the green synthesis of copper and zinc nanoparticles [50,51], but there is no literature on the green synthesis of G-CuO and G-ZnO NPs using the leaves of mallow plants grown in Denizli, indigenous to the Aegean region.

In the present study, I have successfully synthesized CuO and ZnO nanoparticles using mallow plant leaves and observed that CuO nanoparticles can be used as a catalyst. Especially in the synthesis of indole compounds with many applications in the field of medicine, I have obtained high yields in a very short time with the microwave method in a solvent-free environment by using CuO nanoparticles as catalysts. Nanoparticles and bis(indolyl)methanes have been obtained using a cost-effective, economical, environmentally friendly synthesis method that requires very short time.



**Figure 11.** Antibacterial effects of G-CuONPs and G-ZnONPs against *B. subtilis*, *S. Aureus*, *B. Cereus*, *K. pneumoniae*, *V. paraahaemolyticus*, *E. coli*, *S. typhimurium*, *S. enteritis*.

Finally, both CuO and ZnO nanoparticles prepared by green synthesis have significant antibacterial effects and have a lethal effect on some bacteria tested in this study. The results show that CuO and ZnO nanoparticles can possibly be designed as an antibacterial agent that can be used in food protection, pharmaceutical industry, agriculture, and daily use [52,53].

#### Conflict of interest

The author declares no conflicts of interest.

#### Funding

This research did not receive any specific funding.

#### Acknowledgment

I would like to thank Prof. Dr. Ahmet Koluman for supplying bacterial strains required for antibacterial studies and valuable information.

#### References

1. Vijayaraghavan K, Ashokkumar T. Plant-mediated biosynthesis of metallic nanoparticles: a review of literature, factors affecting synthesis, characterization techniques and applications. *Journal of environmental chemical engineering* 2017; 5: 4866-4883. doi: 10.1016/j.jece.201709026
2. Nair V, Abhilash KG, Vidya N. Practical Synthesis of Triaryl- and Triheteroarylmethanes by Reaction of Aldehydes and Activated Arenes Promoted by Gold (III) Chloride. *Organic Letter* 2005; 7: 5857. doi: 10.1021/ol052423h
3. Mishra YK, Adelung R, Röhl C, Shukla D, Spors F et al. Virostatic potential of micro-nano filopodia-like ZnO structures against herpes simplex virus. *Antiviral Research* 2011; 92 (2): 305-12. doi: 10.1016/j.antiviral.201108017
4. Karthik K, Dhanuskodi S, Gobinath C, Prabukumar S, Sivaramakrishnan S. Photocatalytic and antibacterial activities of hydrothermally prepared CdO nanoparticles. *Journal of Materials Science: Materials in Electronics* 2017; 28: 11420–11429. doi: 10.1007/s108540176937z
5. Yeşiltepe D, Gürmen S. Production of nano zinc oxide (ZnO) by hydrothermal method. *TMMOB Metalurji ve Malzeme Mühendisleri Odası Bildiriler Kitabı Uluslararası Metalurji ve Malzeme Kongresi* 2016; 18: 297-299.
6. Verma M, Kumar V, Katoch A. Sputtering based synthesis of CuO nanoparticles and their structural, thermal and optical studies. *Materials Science in Semiconductor Processing* 2018; 76: 55–60. doi: 10.1016/j.mssp.2017.12.018

7. Siddiqui H, Qureshi MS, Haque FZ. Formation of copper oxide nanostructures by solution-phase method for antibacterial application. *International Journal of Scientific & Engineering Research* 2014; 5 (3): 173-177.
8. Zaman S. Synthesis of ZnO, CuO and their Composite Nanostructures for Optoelectronics, Sensing and Catalytic Applications. Linköping University, Physical Electronics and Nanotechnology Department of Science and Technology, Linköping University, Norrköping, Sweden, 2012.
9. Bulcke F, Dringen R. Handling of Copper and Copper Oxide Nanoparticles by Astrocytes. *Neurochem Research* 2016; 41: 33–43. doi: 10.1007/s1106401516889
10. Kholoud MM, Ala' Eftaiha A, Al-Warthan A, Ammar RAA. Synthesis and applications of silver nanoparticles. *Arabian Journal of Chemistry* 2010; 3: 135–140. doi: 10.1016/j.arabjc.201004008
11. Javidan A, Ramezani M, Sobhani-Nasab A, Hosseinpour-Mashkani SM. Synthesis, characterization, and magnetic property of monoferrite BaFe<sub>2</sub>O<sub>4</sub> nanoparticles with aid of a novel precursor. *Journal of Materials Science: Materials in Electronics* 2015; 26: 3813–3818. doi: 10.1007/s1085401529075
12. Saravana Kumar A, Madhan Mohan E. Study on the Anti-Seizure Activity of Methanolic Extracts of *Indigofera Tinctoria* (L.). *Pharmacologyonline*, 2009; 1: 1341-1351.
13. Irvani S. Green synthesis of metal nanoparticles using plants. *Green Chemistry* 2011; 13: 2638-2650. doi: 10.1039/c1gc15386b8
14. Saratale R, Kumar G, Banu R, Xia A, Periyasamy S et al. A critical review on anaerobic digestion of microalgae and macroalgae and co-digestion of biomass for enhanced methane generation. *Bioresource Technology* 2018; 262: 319-332. doi: 10.1016/j.biortech.2018.03.030
15. Makarov VV, Love AJ, Sinitsyna OV, Makarova SS, Yaminsky IV et al. Green Nanotechnologies: Synthesis of Metal Nanoparticles Using Plants. *Acta Naturae* 2014; 6 (1): 35–44
16. Kumar A, Yusuf A, Uttam C, Banerjee C. Synthesis of metallic nanoparticles using plant extracts. *Biotechnology Advances* 2013; 31 (2): 346-356. doi: 10.1016/j.biotechadv.201301003
17. Meydan İ, Seçkin H. Green synthesis, characterization, antimicrobial and antioxidant activities of zinc oxide nanoparticles using *Helichrysum arenarium* extract. *International Journal of Agriculture Environment and Food Sciences* 2021; 5 (1): 33 – 41. doi: 10.31015/jaefs202115
18. Forouzanfar F, Fazly Bazzaz BS, Hosseinzadeh H. Black cumin (*Nigella sativa*) and its constituent (thymoquinone): a review on antimicrobial effects. *Iran Journal Basic Medical Sciences* 2014; 17: 929-938.
19. Murray RDH, Medez J, Brown SA. *The Natural Coumarins: Occurrence, Chemistry and Biochemistry*. New York, NY, USA: Wiley, 1982.
20. Shiri M, Zolfigol M, Kruger HG, Tanbakouchian Z. Bis- and Trisindolylmethanes (BIMsand TIMs). *Chem. Rev* 2010; 110: 2250–2293. doi: 10.1021/cr900195a
21. Abraham R, Prakash P. A novel substrate controlled chemoselective synthesis of aryl bis(thiazole-2-imine)methanes from 2-aminothiazoles and aldehydes. *Tetrahedron Letters* 2017; 58: 3057–3063. doi: 10.1016/j.tetlet.201706068
22. Liao BS, Chen JT, Liu ST. An Efficient Preparation of Bis(indole)methanes Catalyzed by Tetrakis[3,5-bis(trifluoromethyl)phenyl]borate Salts in Aqueous Medium. *Synthesis* 2007; 20: 3125–3128. doi: 10.1055/s2007990788
23. Selvam JJP, Selvam M, Suryakiran, N, Suresh, V, Reddy SM et al. One-Pot Construction of 3,3'-Bisindolylmethanes through Bartoli Indole. *Synthesis Commun* 2008; 38: 1760–1767. doi: 10.1021/o1401486s
24. Wang SY, Ji SJ. Facile Synthesis of Bis(indolyl)methanes catalyzed by Ferric Dodecyl Sulfonate [Fe(DS)<sub>3</sub>] in Water at Room Temperature. *Synthetic Communication* 2008; 38: 1291–1298. doi: 10.1080/00397910701873318
25. Kamble VT, Kadam KR, Joshi NS, Muley DB. Morpholinium bisulfate [morH][HSO<sub>4</sub>]: An efficient and reusable catalyst for the synthesis of bis(indolyl)methanes. *Catalysis Communication* 2007; 8: 498–502. doi: 10.1016/j.catcom.200607010
26. Seyed H, Maryam A. Synthesis and characterization of polyindole with liquid crystalline azobenzene as side chains. *Journal of Physical Science* 2013; 8 (32): 1611-1622. doi: 10.5897/ijps12107
27. Nair V, Abhilash KG, Vidya N. Practical Synthesis of Triaryl- and Triheteroarylmethanes by Reaction of Aldehydes and Activated Arenes Promoted by Gold (III) Chloride, *Organic Letter* 2005; 7: 5857. doi: 10.1021/ol052423h
28. De ML, Bhuyan PJ. An efficient and clean synthesis of bis(indolyl)methanes in a protic solvent at room temperature. *Tetrahedron Letter* 2006; 47: 1441–1443. doi: 10.1080/14756360802292974
29. Paola P, Vittorio L, Antonietta Zoroddu M, Gavina M, Salvatore D et al. Complexes of indole-3-carboxylic, indole-3-acetic, indole-3-β-acrylic, indole-N-acetic and indole-N-methyl-2-carboxylic acids with some divalent metal ions. *Transition Metal Chemistry* 1992; 17 (4): 283-286. doi: 10.1007/bf02910889
30. Firouzabadi H, Iranpoor N, Jafarpour M, Ghaderi M. ZrOCl<sub>2</sub>·8H<sub>2</sub>O/silica gel as a new efficient and a highly water-tolerant catalyst system for facile condensation of indoles with carbonyl compounds under solvent-free conditions. *Journal of Molecular Catalysis A: Chem* 2006; 253: 249–251. doi: 10.1016/j.molcata.200603043

31. Mona HS. Synthesis of Bis(indolyl)methanes using a Catalytic Amount of ZnO under Solvent-Free Conditions. *Synthetic Communications* 2008; 38: 832–840. doi: 10.1080/00397910701845274
32. Ghaderi BM, Reddy P, Sreekanth M, Pandian L. Room-Temperature Synthesis of Diindolylmethanes Using Silica-Supported Sulfuric Acid as a Reusable Catalyst Under Solvent-Free Conditions *Journal of Molecular Catalysis A: Chem* 2005; 237: 93–100. doi: 10.1080/003979112010505696
33. Qia L, Xiaoa L. Convenient Synthesis and Anticancer Activity of Bis(aryl)alkanes and Bis(indolyl)methane Alkaloid Analogs. *Russian Journal of General Chemistry* 2020; 90 (10): 1974–1980. doi: 10.1134/s1070363220100217
34. [34] Bahea AK, Dasa R, Naikoob GA, Kostia P, Kashawc S. Antibacterial Activity of Bis(Indolyl) Methane Derivatives against *Staphylococcus Aureus* *Advanced Journal of Chemistry-Section A* 2020; 3 (6): 722-729 doi: 10.22034/ajca2020106912
35. Hermkens PHH, Ottenheijm HCJ, Ress DC. Solid-phase organic reactions II: A review of the literature Nov 95-Nov 96. *Tetrahedron* 1997; 53 (16): 5643-5678. doi: 10.1016/S00404020(97)002792
36. Perreux L, Loupy A. A tentative rationalization of microwave effects in organic synthesis according to the reaction medium, and mechanistic considerations. *Tetrahedron* 2001; 57 (45): 9199-9223. doi: 10.4236/amp201321012 P
37. Lindström P, Tierney J, Wathey B, Westman J. Microwave assisted organic synthesis-a review, *Tetrahedron* 2001; 57: 9225-9283. doi: 10.1016/S00404020(01)009061
38. Chand K, Cao D, Eldin Fouad D, Shah AH, Qadeer Dayo A et al. Green synthesis, characterization and photocatalytic application of silver nanoparticles synthesized by various plant extracts. *Arabian Journal of Chemistry* 2020; 13 (11): 8248-8261. doi: 10.1016/j.arabjch.2020.1009
39. Mohammad WA, Akl MA. Green synthesis of copper nanoparticles by Citrus limon fruits extract, characterization and antibacterial activity. *Chemistry International* 2021; 7 (1): 1-8. doi: 10.5281/zenodo.4017993
40. Shah M, Fawcett D, Sharma S, Tripathy SK, Poinern GEJ. Green synthesis of metallic nanoparticles via biological entities. *Materials* 2015; 8: 7278–7308. doi: 10.3390/ma8115377
41. Dhineshbabu NR, Rajendran NR, Nithyavathy N, Vetumperumal R. Study of structural and optical properties of cupric oxide nanoparticles *Applied Nanoscience* 2016; 6: 933–939 doi: 10.1007/s1320401504992
42. Nagarajan R, Perumal PT. Potassium hydrogen sulfate-catalyzed reactions of indoles: a mild, expedient synthesis of bis-indolylmethanes. *Chemistry letters* 2004; 33 (3): 288-289. doi: 10.1246/cl2004288
43. Sintubin L, Verstraete W, Boon N. Biologically produced nanosilver: Current state and future perspectives. *Biotechnology Bioengineering* 2012; 109 (10): 2422–2436. doi: 10.1002/bit24570
44. Patterson A. The Scherrer Formula for X-Ray Particle Size Determination. *Physical Review* 1939; 56 (10): 978–982. doi: 10.1103/PhysRev.56.978
45. Baker S, Rakshith D. Plants: Emerging as nanofactories towards facile route in synthesis of nanoparticles. *BioImpacts* 2013; 3: 111–117. doi: 10.5681/bi2013012
46. Essic J, Mather R. Characterization of a bulk semiconductors band gap via near- absorption edge optical transmission experiment. *American Journal of Physics* 1993; 61: 646–649. doi: 10.1119/117173
47. Dharma J, Pisa A, Shelton C. Simple method of measuring the band gap energy value of TiO<sub>2</sub> in the powder form using a UV/Vis/NIR spectrometer. *Application Note, Shelton, CT USA PerkinElmer*, 2016.
48. Mukherjee S, Sushma V, Patra S, Barui AK, Pal Bhadra M et al. Green chemistry approach for the synthesis and stabilization of biocompatible gold nanoparticles and their potential applications in cancer therapy. *Nanotechnology*. 2012; 23 (45): 455103. doi: 10.1088/095744842345455103
49. Azam A, Ahmed AS, Oves M, Khan MS et al. Antimicrobial activity of metal oxide nanoparticles against Gram-positive and Gram-negative bacteria: a comparative study *International Journal of Nanomedicine*. 2012; 7: 6003–6009. doi: 10.2147/IJNS35347
50. Sylvia Devi H and David Singh T. Synthesis of Copper Oxide Nanoparticles by a Novel Method and its Application in the Degradation of Methyl Orange. *Advance in Electronic and Electric Engineering* 2014; 4 (1): 83-88.
51. Shah M, Fawcett D, Sharma S, Tripathy SK and Poinern GEJ. Green synthesis of metallic nanoparticles via biological entities. *Materials* 2015; 8: 7278–7308. doi: 10.3390/ma8115377
52. Li W, Xie X, Shi Q, Duan S, Ouyang YS et al. Antibacterial effect of silver nanoparticles on *Staphylococcus aureus*. *Biometals* 2011; 24: 135–141. doi: 10.1007/s1053401093816
53. Sevinç BA and Hanley L. Antibacterial activity of dental composites containing zinc oxide nanoparticles. *Journal of Biomedical Materials Research* 2010; 94 (1): 22–31. doi: 10.1002/jbmb31620